2023-2024

CARNATIONS PROJECT 6 SYNOPSIS

MULTI-VEHICLE/INFRASTRUCTURE JAMMER/SPOOFER DETECTION AND LOCALIZATION

DEPARTMENT OF TRANSPORTATION UNITED STATES OF AMERICA
ILLINOIS TECH
CHICAGO STATE UNIVERSITY
UC RIVERSIDE
Stanford
VIRGINIA TECH

Exhibit C

Technical Report Documentation Form, DOT F 1700.7

DISCLAIMER:

Technical Report Documentation

<table>
<tr><td>1. Report No.
6</td><td>2. Government Accession No.
N/A</td><td>3. Recipient's Catalog No.
N/A</td></tr>
<tr><td colspan="2" rowspan="2">4. Title and Subtitle
Multi-Vehicle/Infrastructure Jammer/Spoofer Detection and Localization</td><td>5. Report Date
10/1/2023 – 9/30/2024</td></tr>
<tr><td>6. Performing Organization Code
n/a</td></tr>
<tr><td colspan="2">7. Author(s)
• Matthew Barth https://orcid.org/0000-0002-4735-5859
• Jay Farrell https://orcid.org/0000-0002-2077-8691
• Mathieu Joerger https://orcid.org/0000-0002-6391-9095
• Hang Qiu https://orcid.org/0000-0003-1206-9032
• Saswat Priyadarshi Nayak https://orcid.org/0000-0003-2210-0021
• Guoyuan Wu https://orcid.org/0000-0001-6707-6366
• Zhengwei Bai https://orcid.org/0000-0002-4867-021X</td><td>8. Performing Organization Report No.
6</td></tr>
<tr><td colspan="2" rowspan="2">9. Performing Organization Name and Address
University of California, Riverside, 900 University Ave, Riverside, CA 92521

Virginia Polytechnic Institute and State University
Blacksburg, VA 24061-0002</td><td>10. Work Unit No.</td></tr>
<tr><td>11. Contract or Grant No.
Illinois Institute of Technology/69A3552348324</td></tr>
<tr><td colspan="2" rowspan="2">12. Sponsoring Agency Name and Address

Office of the Assistant Secretary for Research and Technology, University Transportation Centers Program, Department of Transportation, Washington DC, 20590, United States</td><td>13. Type of Report and Period Covered
Final Report 10/1/2023 – 9/30/2024</td></tr>
<tr><td>14. Sponsoring Agency Code
USDOT, OST-R</td></tr>
<tr><td colspan="3">15. Supplementary Notes
Conducted in cooperation with the U.S. Department of Transportation, Federal Highway Administration.</td></tr>
</table>

16. Abstract

This project followed three paths in parallel, all focused on developing vehicle strategies that provide improved knowledge of and resilience to positioning uncertainty, in particular, of the potential risk of spoofing. The first path is focused on developing resilient connected and automated vehicle (CAV) applications given uncertain PNT services; the second is developing resilience techniques through a multi-agent community approach; and the third is to conduct research on collaborative radio-frequency interference (RFI) localization.

1. The focus of the first research path is to develop CAV applications that are "aware" of their positioning uncertainty and the potential risk of spoofing and adapt to make them more robust in terms of safety, mobility, and environmental factors. This research consists of several tasks, including: 1) searching CAV application literature to identify any applications that are adaptable in terms of positioning and spoofing uncertainty; 2) identifying a variety of CAV fundamental maneuvers that can be targeted for position uncertainty adaptive algorithms; 3) designing these adaptive algorithms for a subset of fundamental maneuvers (e.g. vehicle merging), followed by comprehensive testing both in simulation and in the real world; and 4) developing the means for estimating and communicating position uncertainty and the risk of undetected spoofed PNT services.

2. The focus of the second research path is to develop resiliency techniques using a multi-agent community approach where a diversity of connected vehicles and infrastructure are operating in close proximity. Within this community, the impacts of jamming can be mitigated by community alerts directing vehicles to switch to non-GNSS PNT or to avoid a particular area. During spoofing, the spoofed GNSS signals can be generated based on only one vehicle's predicted trajectory; however, spoofed signals are received by all vehicles within a given neighborhood of the broadcaster. All other vehicles within the reception volume are receiving inconsistent GNSS signals, which enables community detection of spoofing. This research aims at quantifying the performance of this detection approach and at analyzing the impact of transportation threats in several scenarios.

3. In the third research path, we demonstrate the ability of multiple connected vehicle receivers to detect and localize a common RFI source. We determine the circumstances under which such a collaborative RFI detection and localization scheme are possible. For example, if two receivers are within reach of an RFI source, using time-differenced measurements over larger than 100-meter separation distances can enable time-of-arrival localization. Phase differences can be more challenging to achieve but reduce the baseline requirement to meter level. The research path aims at quantifying the resulting localization performance in example use-cases.

17. Key Words	**18. Distribution Statement**
Positioning Uncertainty, Spoofing, Connected and Automated Vehicles (CAV), Resilience, Radio-Frequency Interference (RFI), Multi-agent Community, GNSS, PNT Services, Localization, Detection, Adaptive Algorithms, Community Alerts, Jamming, Trajectory, Time-of-arrival Localization, Phase Differences, Transportation Threats, Safety, Mobility, Environmental Factors, Simulation.	No restrictions. This document is available through the National Technical Information Service, Springfield, VA 22161. Enter any other agency mandated distribution statements. Remove NTIS statement if it does not apply.

19. Security Classif. (of this report)	**20. Security Classif. (of this page)**	**21. No. of Pages**	**22. Price**
Unclassified	Unclassified	6	

Form DOT F 1700.7 (8-72) Reproduction of completed page authorized

CARNATIONS
Year 1 Project 6 (2023-2024)
Multi-Vehicle/Infrastructure Jammer/Spoofer Detection and Localization, Year 1

Recipient/Grant Number: Illinois Institute of Technology/69A3552348324

Center Name: Center for Assured and Resilient Navigation in Advanced Transportation Systems (CARNATIONS)

Research Priority: Reducing Transportation Cybersecurity Risks

Principal Investigators: Matthew Barth, UC Riverside; Co-PI: Jay Farrell, UC Riverside

Other Investigator(s): Co-PIs: Matthew Spenko, Mathieu Joerger

Direct costs billed to CARNATIONS project and cost sharing: UCR: $135,837; cost share: $67,918

Reporting period start and end date: 10/1/2023 – 9/30/2024

Project goals summary from original proposal: The main focus of the first research path is to develop CAV applications that are "aware" of their positioning uncertainty and the potential risk of spoofing, and adapt to make them more robust in terms of safety, mobility, and environmental factors. This consisted of several tasks, including: 1) carrying out a CAV application literature search to identify any applications that are adaptable in terms of positioning and spoofing uncertainty; 2) identifying a variety of CAV fundamental maneuvers that can be targeted for position uncertainty adaptive algorithms; 3) designing these adaptive algorithms for a subset of fundamental maneuvers (e.g. vehicle merging), followed by comprehensive testing both in simulation and in the real world; and 4) developing the means for estimating and communicating position uncertainty and the risk of undetected spoofed PNT services.

Technical summary of major project achievements for the year and project outputs: In this first-year jump start project, we reviewed multiple works focused on ensuring accurate and reliable positioning for Connected and Automated Vehicle (CAV) applications, particularly for safety-critical functions. As CAV technologies continue to evolve, maintaining precise and resilient positioning has become crucial for applications like collision avoidance and autonomous intersection management. Our review highlighted the roles of perception sensors such as cameras and LiDAR, as well as Vehicle-to-Vehicle (V2V) and Vehicle-to-Infrastructure (V2I) communication systems, in enhancing positioning accuracy in mixed traffic environments. As part of this review, we created the topology shown in Figure 1. Despite these advancements, we identified a significant need to develop a robust integrity monitoring (IM) framework to ensure the reliability of positioning data across diverse traffic conditions.

As part of this project, we identified several challenges associated with positioning in mixed traffic conditions. In these scenarios, a wide variety of vehicles — from human-driven vehicles (HDVs) to connected vehicles (CVs) and automated vehicles (AVs) — coexist, each equipped with different sensor suites and computational capabilities. This diversity leads to inconsistencies in positioning accuracy and performance, complicating the task of maintaining reliable data integrity. Moreover, we found that environmental factors, such as urban canyons that can obstruct signals, and the presence of vulnerable road users (VRUs) with limited or varying positioning capabilities, further complicate the challenge of achieving robust positioning integrity monitoring.

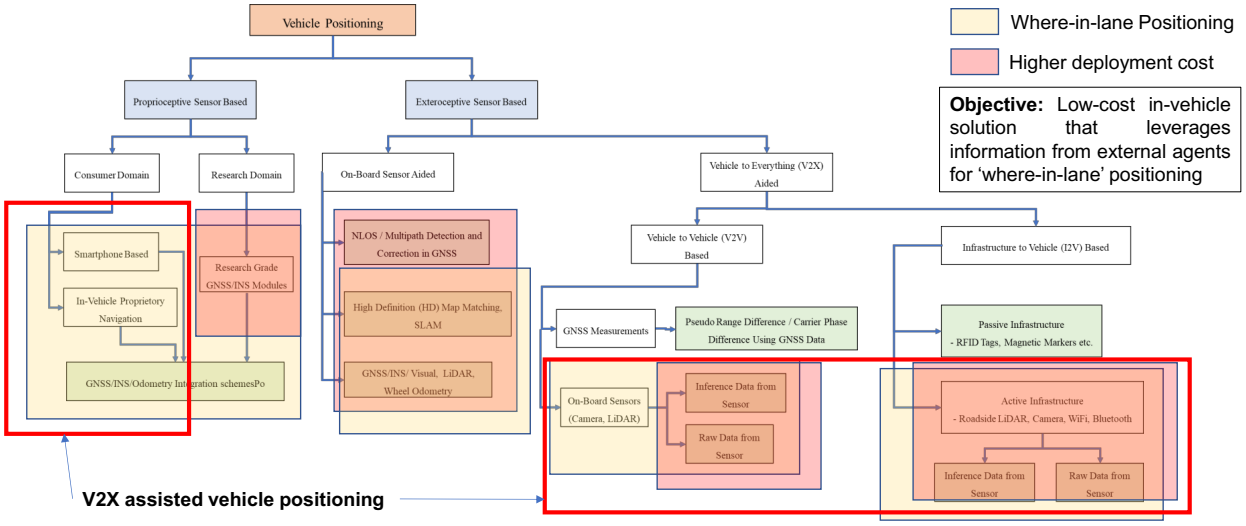

Figure 1: V2X-Assisted Positioning Topology

To address these challenges, we conducted a comprehensive review of existing integrity monitoring frameworks, both standalone (in-vehicle) and cooperative (involving multiple vehicles or infrastructure). We found that standalone IM methods, such as Receiver Autonomous Integrity Monitoring (RAIM), Kalman filters, and cross-consistency checks, are widely used for fault detection within a single vehicle's sensor system. However, cooperative IM approaches, which involve sharing data between vehicles and infrastructure to enhance overall positioning reliability, are still in their early stages. Our review, illustrated in Figure 2, indicates that there are limited studies that thoroughly address the complexities involved in multi-source data sharing and the integrity risks that arise from wireless communication between different road agents. However, it is clear that cooperative perception shows great promise for improving positioning reliability and resiliency.

Sensor Type	Positioning Solution	Use	Validation	Cost	CAV Penetration*	Accuracy
Proprioceptive Sensors	GNSS/INS/Wheel Odometry Integration Schemes In-use*	Operational	In-field	Low	Independent	3-5 m (GNSS) < 1 m (Augmentation)
Standalone / Exteroceptive Sensors	**On-board Sensor Aided** A. NLOS / Multipath detection and Correction w/ camera & LiDAR B. High-Definition Maps, SLAM C. GNSS/INS/Visual-LiDAR-Wheel Odometry	R & D** Operational Operational	In-field	High High Medium	Independent	~ 19 m (Deep Urban Canyon) < 1 m 40 -75 % Improvement over traditional GNSS/INS/RTK
Cooperative	**Vehicle-to-Vehicle Based (V2V)** A. GNSS measurement – Pseudorange/Carrier Phase difference B. On-board sensor data sharing	R & D R & D	Mostly In-simulation	Low High	> 30 %	~ 0.8 – 1.3 m
Cooperative	**Infrastructure-to-Vehicle Based (I2V)** A. Passive Infrastructure – Magnetic markers, RFID, etc. B. Active Infrastructure – Roadside Camera/LiDAR/WiFi/BLE Promising*	Operational R & D	In-field Mostly In-simulation	Medium High **(Infrastructure Cost)**	Independent	1 – 2 m < 1 m

*CAV Penetration – Percentage of CAVs in the traffic, **R & D – Research and Development

Figure 2: Standalone and Cooperative Positioning Solutions

As an example of V2V cooperative perception, we have conducted experiments identifying other vehicles around an ego-vehicle, as shown in Figure 3 (from [3]). As an example of V2I cooperative perception, the research team has carried out a variety of experiments on Riverside's Innovation Corridor (https://www.cert.ucr.edu/riverside-innovation-corridor), illustrated in Figure 4.

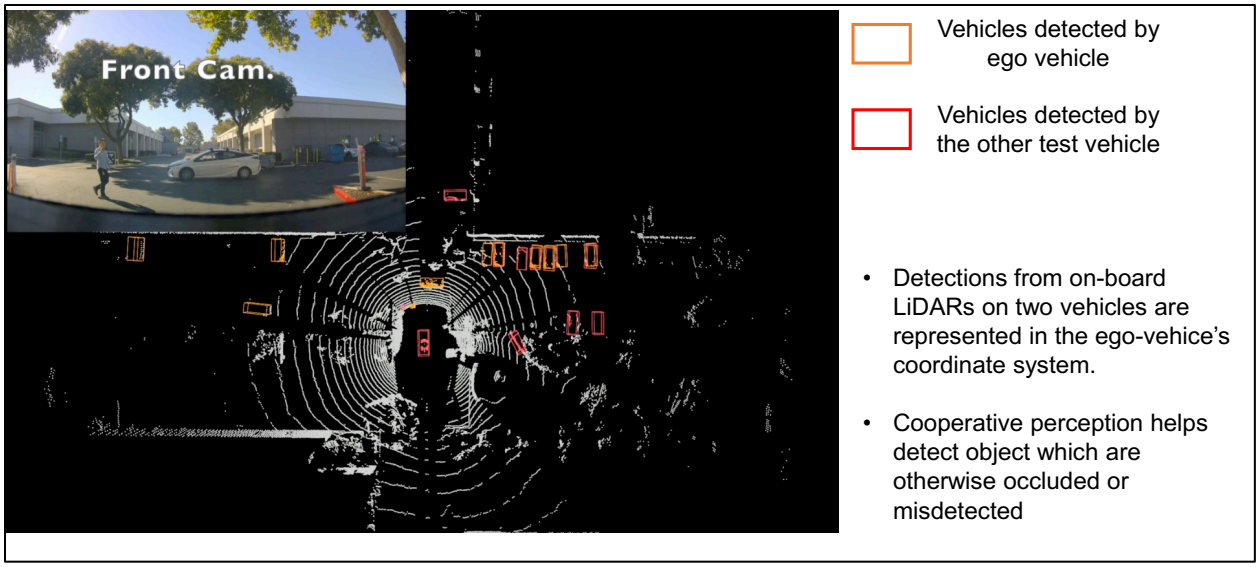

Figure 3: Example of V2V cooperative perception conducted by research team (from [2])

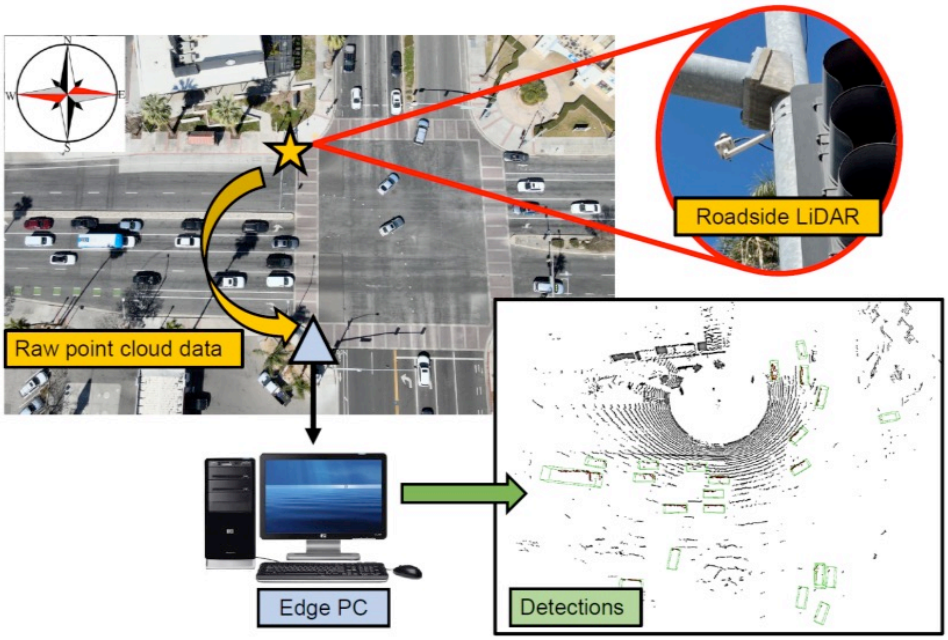

Figure 4: Example of V2I cooperative perception (using LiDAR) conducted by research team (from [1, 3])

Based on our findings, we identified several key areas for improvement in existing IM frameworks. For instance, we propose introducing new evaluation parameters such as timeliness and interoperability to better assess the performance of cooperative ITS applications. Additionally, we emphasize the importance of conducting hardware-in-the-loop simulations to test various sensor modalities and driving conditions that are difficult to replicate in real-world scenarios. This approach would allow us to explore different configurations and failure modes in a controlled environment, accelerating the development of robust IM methods. We also recognized the need to standardize the required navigation performance (RNP) values across different CAV applications to ensure consistency and interoperability among diverse vehicles and systems, which would be essential for the widespread adoption of these technologies.

In parallel, the Illinois Tech (PI: Spenko) and Virginia Tech (PI: Joerger) teams met weekly to evaluate collaborative Kalman-filter-based LiDAR/inertial navigation integrity monitoring methods. We showed using simulation and experimental data that combining LiDAR/IMU measurements from multiple vehicles improves accuracy, which was to be expected. The integrity performance, however, depends on the accuracy and failure rate of the inter-vehicle link. Field testing was performed using two cars equipped with tightly-integrated LiDAR/inertial systems, with real-time kinematic (RTK) GNSS for ground truth, and with retro-reflective markers. Integrity performance was significantly improved for the collaborative versus individual vehicle implementation in the along-track direction. This research is described in detail in Appendix A of this report. Additional research is needed to achieve significant improvement in the cross-track direction, which is needed in lane following operations.

In conclusion, our work in this first-year jump-start project has identified several gaps in the existing integrity monitoring methods, particularly for cooperative environments where vehicles must share and trust each other's data. We believe further research is necessary to address these challenges and enhance the safety and reliability of CAV applications. Moving forward, we plan on conducting new research projects to develop more sophisticated algorithms for data fusion and fault detection and create standardized performance metrics to improve positioning integrity in mixed traffic scenarios. These efforts are directly aligned with our goal of developing a robust framework for multi-object tracking and positioning in low-data-rate environments, which is crucial for the future of cooperative positioning systems.

Ways that the project has contributed to CARNATIONS goals and US DOT Priorities:

The project has made substantial contributions to the goals of the CARNATIONS initiative and the U.S. Department of Transportation (US DOT) priorities by pioneering innovative positioning integrity monitoring solutions. These advancements play a crucial role in enhancing the safety of transportation systems, fostering technological innovation, improving infrastructure efficiency, promoting environmental sustainability, and ensuring equity across all modes of transportation. By developing methods to deliver accurate and reliable positioning data for Connected and Automated Vehicles (CAVs) operating in mixed traffic environments, the project supports safety-critical applications such as collision avoidance systems and autonomous intersection management. This aligns closely with the US DOT's Vision Zero goal of eliminating traffic fatalities and serious injuries on American roads.

Moreover, the project's emphasis on cooperative data sharing and multi-source data integration strengthens a connected transportation ecosystem. This fosters improved traffic management by optimizing traffic flow, reducing congestion, and lowering emissions, thereby contributing to the US DOT's sustainability goals. Furthermore, by promoting an inclusive network that integrates diverse transportation modes and serves all communities equitably, including those that have been traditionally underserved, the project aligns with the US DOT's commitment to equity in transportation. This focus on inclusivity ensures that the benefits of technological innovation and sustainable development reach every part of society, supporting broader social and economic development objectives.

Contributions to CARNATIONS project's research performance metrics: Research articles [1,2,3] were presented in conferences and published in peer-reviewed journals.

Contributions to CARNATIONS project's tech transfer and education performance metrics: Several posters and presentations related to this project were made at the 2024 IEEE Forum for Innovative Sustainable Transportation Systems (FISTS24), held in February 2024. This conference was attended by academics (faculty, students), industry members, and members from various government agencies.

References

1. Nayak, Saswat Priyadarshi, Wu, Guoyuan, Barth, Matthew, Liu, Yongkang, Sisbot, Emrah Akin, Oguchi, Kentaro, "Infrastructure-Assisted Cooperative State Estimation of Ego-Vehicle via Augmentation of Asynchronous Kinematic Measurements," *Proceedings of the 2024 International Technical Meeting of The Institute of Navigation*, Long Beach, California, January 2024, pp. 1103-1116. https://doi.org/10.33012/2024.19537

2. Bai, Z., Wu, G., Barth, M. J., Qiu, H., Liu, Y., Sisbot, E. A., & Oguchi, K. (2024). "Pillar Attention Encoder for Adaptive Cooperative Perception", *IEEE Internet of Things Journal*, 11(14), 24998–25009. https://doi.org/10.1109/jiot.2024.3390552.

3. Nayak, Saswat Priyadarshi, Wu, Guoyuan, Barth, Matthew, Liu, Yongkang, Sisbot, Emrah Akin, Oguchi, Kentaro, "Evaluation of Infrastructure-Assisted Cooperative Tracking of Vehicles Using Various Motion Models," *2023 IEEE/ION Position, Location and Navigation Symposium (PLANS)*, Monterey, CA, April 2023, pp. 243-253. https://doi.org/10.1109/PLANS53410.2023.10139968

Appendix A. Impact of Sensor Faults on Connected Autonomous Vehicle Localization

Shinsaku Kuwada (Illinois Tech), Matthew Spenko (Illinois Tech), and Mathieu Joerger (Virginia Tech)

A-1. Introduction

Precise localization and predictable localization error bounding are crucial to mobile robot safety. However, achieving this is challenging because robots typically rely on exteroceptive sensors such as GNSS, cameras, LiDAR, and radar that may experience undetected faults and unpredictable interference due to jamming and collateral spoofing. This project focuses on LiDAR/inertial navigation to augment positioning, navigation and timing (PNT) in areas where GNSS service might be denied. It shows that, in case of LiDAR measurement or processing faults, collaboration and communication among connected autonomous vehicles (CAVs) can enhance navigation safety.

A system of multiple CAVs can be categorized as either centralized or decentralized, and is similar to a multi-robot collaboration scenario, where much of the literature exists. In a centralized system, a single hub manages all robots' information. A centralized approach is impractical for large numbers of robots. In contrast, a decentralized system considers smaller groups of robots, making it more scalable, but the challenge is then to accurately capture inter-group correlations. In both approaches, collaborative localization allows a CAV to access information that would otherwise be unavailable, thereby enhancing its estimation accuracy.

Unfortunately, collaboration also introduces risks. If a robot with faulty sensor data shares incorrect information, it can compromise other robots' localization accuracy. Moreover, if communication is maliciously spoofed, the resulting collaborative position and orientation (or pose) estimates can be corrupted.

Navigation safety for a mobile robot is typically assessed considering its sample estimation error and covariance [A1]. These metrics are insufficient when considering the possibility of rarely-occurring, undetected sensor and processing faults. Fault detectors can be implemented to exclude measurements or raise alerts [A2], but there is still a risk that undetected faults impact the pose estimation error. To address this, methods developed in GNSS-based navigation safety can be leveraged: integrity monitoring can be used to evaluate the effects of undetected sensor measurement faults on pose estimation [A3, A4, A5].

Previous work evaluated the impact of undetected sensor measurement faults on a single robot's localization in GNSS-denied environments [A6, A7, A8, A9]. However, there has been limited analysis on the effect of such faults on collaborative localization. In [A10], a fault detector using GNSS measurements from multiple CAVs identified common GNSS satellite faults. Building on this, reference [A11] enhanced the fault detector performance by incorporating CAV collaboration, enabling the detection of GNSS faults and faults in inter-vehicle relative measurements. While these approaches achieved notable results by leveraging CAV collaboration, they focus on improving CAV fault detectors and do not address undetected faults, a critical component of integrity analysis [A12].

To analyze the impact of undetected faults on multi-robot navigation systems, this project extends an integrity monitoring approach based on previous work to multi-robot systems by assessing the impacts of undetected sensor measurement and processing faults on collaborative localization for both centralized and decentralized systems.

A-2. Problem Statement: Assumptions and Assertions

State Propagation and Measurement Model

Consider a system of N homogeneous robots: $\mathcal{R} = \{R_i \mid 1 \leq i \leq N,\ i \in N\}$ where R_i represents the i^{th} robot. Given a robot's state at epoch k, $x_k \in \mathbb{R}^m$, the state evolution model is given by:

$$\boldsymbol{x_k^i} = \boldsymbol{g}\left(\boldsymbol{x_{k-1}^i}, \boldsymbol{u_{k-1}^i}\right) + \boldsymbol{w_{k-1}^i} \tag{1}$$

where u_{k-1}^i is the control input, $g(\cdot,\cdot)$ is a nonlinear state evolution function, and $w_{k-1}^i \sim \mathcal{N}\left(0, W_{k-1}^i\right)$ is a Gaussian disturbance with known covariance W_{k-1}^i. To be more accurate, w_{k-1}^i does not have to follow a Gaussian distribution, but we assume that it is overbounded by a Gaussian function $\mathcal{N}\left(0, W_{k-1}^i\right)$ [A4,A 6-10]. If R_i detects n_k^i landmarks at epoch k, each with m_F measurable features, the measurement vector of R_i is denoted as:

$$\boldsymbol{z_k^i} = \begin{bmatrix} \boldsymbol{z_{k,1}^T} & \cdots & \boldsymbol{z_{k,n_k^i}^T} \end{bmatrix}^T \in \mathbb{R}^{n_k^{F,i}} \tag{2}$$

where $n_k^{F,i} = n_k^i m_F$.

The measurement model is given by:

$$\boldsymbol{z_k^i} = \boldsymbol{h}\left(\boldsymbol{x_k^i}\right) + \boldsymbol{v_k^i} + \boldsymbol{f_k^i} \tag{3}$$

where $h(\cdot)$ is a nonlinear measurement function, $v_k^i \sim \mathcal{N}\left(0, V_k^i\right)$ is Gaussian white noise with known covariance V_k^i, and f_k^i is a vector of unknown measurement faults that is zero if all measurements are fault-free. Similar to w_{k-1}^i, v_k^i does not have to follow a Gaussian distribution, but we assume that it is overbounded by a Gaussian function $\mathcal{N}\left(0, V_k^i\right)$. Faults can occur when extracted features are incorrectly associated with non-corresponding mapped landmarks (misassociation) or when an unmapped object is associated with a mapped landmark (unmapped association). We assume that only unmapped association faults are present and leave misassociation faults to future work.

Similarly, if the i^{th} robot detects observable features, such as relative position and velocity, of another robot, R_j, at epoch k, the relative measurement vector from R_i to R_j, $z_k^{i\to j} \in \mathbb{R}^{n_k^{i\to j}}$ is modeled as:

$$\boldsymbol{z_k^{i\to j}} = \boldsymbol{h^{i\to j}}\left(\boldsymbol{x_k^i}, \boldsymbol{x_k^j}\right) + \boldsymbol{v_k^{i\to j}} + \boldsymbol{f_k^{i\to j}} \tag{4}$$

where $h^{i\to j}(\cdot,\cdot)$ is a nonlinear relative measurement function, $v^{i\to j} \sim \mathcal{N}\left(0, V_k^{i\to j}\right)$ is overbounded by a Gaussian function with known covariance $V_k^{i\to j}$, and $f_k^{i\to j}$ is a vector of unknown relative measurement faults.

Incorrect relative measurement associations are less common than incorrect landmark measurement associations because CAVs are typically equipped with radios that transmit detailed information that improve association accuracy [A13]. Relative measurement faults are more likely due to external factors such as multi-path interference [A14], communication delays [A15], or a biased state estimate of the observed robot.

We assume that relative measurement faults are not caused by the estimation bias of other robots to ensure consistency in each robot's estimation [A16, A17].

Collaborative Integrity Monitoring Assumptions

If each robot's state estimate error distribution can be overbounded by a Gaussian function or approximated to be normally distributed with respect to its estimate, then the distribution may be biased if measurement faults are present in (3) and (4):

$$\delta\hat{\boldsymbol{x}} = \hat{\boldsymbol{x}} - \boldsymbol{x} \sim \mathcal{N}\left(\boldsymbol{f_{\hat{x}}}, \hat{\boldsymbol{P}}\right) \tag{5}$$

where $f_{\hat{x}}$ represents the unknown estimation bias. If such a bias exists, the estimation may not be consistent, i.e., it is not guaranteed to converge [A18, A19], highlighting the need for monitoring such faults. This can be achieved by introducing a fault detector constructed from test statistics (e.g., estimation error or measurement vector). Faults that cause considerable estimation bias can be easily detected. However, there remains a small, but non-negligible, probability that a non-zero number of measurement faults go undetected despite causing bias in the estimation. Small faults might not cause significant estimation divergence, but they can still have a strong impact on the resulting estimation. Thus, it is important to analyze situations where the fault detector is not triggered but the estimation error exceeds a predefined threshold (known as Hazardous Misleading Information (HMI)).

To quantify the impact of such events, the probability of HMI, or integrity risk, is defined as:

$$P(HMI_k) = P\left(\delta\widehat{\boldsymbol{x}_k} > l \cap q_k < T_{D_k}\right) \tag{6}$$

where $\delta\hat{x}$ represents the estimation error, l is a predefined acceptable error threshold, q is the fault detector, and T_D is the detector threshold such that when $q_k \geq T_{D_k}$ an alarm is triggered.

Since both the estimation error and fault detector are affected by measurement faults, integrity risk is evaluated under several fault hypotheses that specify which set of measurements might be faulted. Given a set of mutually exclusive and collectively exhaustive fault hypotheses, $\{H_0, \cdots, H_{n_H}\}$, the integrity risk at epoch k is defined as:

$$P(HMI_k) = \sum_{h=0}^{n_H} P(HMI_k|H_h)P(H_h) \tag{7}$$

where $P(H_h)$ is the probability of the h^{th} hypothesis, n_H is the total number of fault hypotheses, and H_0 is the fault-free hypothesis. [20] describes how to quantify this probability given the probability of each measurement being faulted.

To evaluate the integrity risk in (6), both the estimation error and the fault detector's distributions must be derived. The remainder of the report presents these distributions for both centralized and decentralized CAV systems.

A-3. Collaborative Estimator Design: Two Approaches

Centralized Extended Kalman Filter

Here, we use the Centralized Extended Kalman Filter (CEKF) for the centralized system's estimator because it can explicitly and analytically track the inter-robot cross-correlations through first-order approximations, unlike other nonlinear estimators such as the Particle Filter [A21]. Given $\mathcal{R}$, the joint state and its covariance for robots in $\mathcal{R}$ are:

$$\boldsymbol{x} = \left[\boldsymbol{x^{1}}^T \cdots \boldsymbol{x^{i}}^T \cdots \boldsymbol{x^{N}}^T\right]^T \tag{8}$$

$$\boldsymbol{P} = \begin{bmatrix} \boldsymbol{P_{11}} & \boldsymbol{P_{12}} & \cdots & \boldsymbol{P_{1N}} \\ \boldsymbol{P_{21}} & \boldsymbol{P_{22}} & \cdots & \boldsymbol{P_{2N}} \\ \vdots & \vdots & \ddots & \vdots \\ \boldsymbol{P_{N1}} & \boldsymbol{P_{N2}} & \cdots & \boldsymbol{P_{NN}} \end{bmatrix} \tag{9}$$

where x^i is the state of R_i, P_{ii} or P_i is the covariance of R_i's state estimate, and P_{ij} is the cross-covariance between R_i and R_j $(i \neq j)$. With this joint state and covariance, the CEKF prediction and update steps are formulated similarly to the EKF [A22]:

$$\bar{\boldsymbol{x}}_k = g(\hat{\boldsymbol{x}}_{k-1}, \boldsymbol{u_{k-1}}) \tag{10}$$

$$\bar{\boldsymbol{P}}_k = \boldsymbol{G_k}\hat{\boldsymbol{P}}_{k-1}\boldsymbol{G_k^T} + \boldsymbol{W_k} \tag{11}$$

$$\hat{\boldsymbol{x}}_k = \bar{\boldsymbol{x}}_k + \boldsymbol{K_k}\boldsymbol{\gamma_k} \tag{12}$$

$$\hat{\boldsymbol{P}}_k = (\boldsymbol{I} - \boldsymbol{K_k}\boldsymbol{H_k})\bar{\boldsymbol{P}}_k \tag{13}$$

where $\gamma_k = z_k - h(\bar{x}_k)$ is the joint innovation, $K_k = \bar{P}_k H_k^T Y^{-1}$ is the Kalman gain, $Y_k = H_k \bar{P}_k H_k^T + V_k$ is the covariance of the joint innovation, and G_k and H_k are the joint Jacobians for $g(\cdot,\cdot)$ and $h(\cdot)$, respectively.

The full form of the joint motion Jacobian G is:

$$\boldsymbol{G} = diag(\boldsymbol{G_1}, \cdots, \boldsymbol{G_i}, \cdots, \boldsymbol{G_N}) \tag{14}$$

where $G_i = \partial g\left(\hat{x}^i, u^i\right) / \partial x^i$ and $diag(\cdot)$ denotes a block diagonal matrix.

The joint measurement vector is assumed to be:

$$\boldsymbol{z_k} = \underbrace{\left[\cdots \boldsymbol{z_k^{i^T}} \cdots\right.}_{LM} \underbrace{\cdots \boldsymbol{z_k}^{\boldsymbol{i\to j^T}} \cdots \left.\right]^T}_{RM} \tag{15}$$

where LM represents landmark measurements and RM represents relative measurements. Accordingly, the joint measurement Jacobian H is:

$$\boldsymbol{H} = \left[\cdots \boldsymbol{H_{ii}}^{\boldsymbol{T}} \cdots \boldsymbol{H_{ij}}^{\boldsymbol{T}} \cdots\right]^T \tag{16}$$

where

$$\boldsymbol{H_{ii}} = \left[\boldsymbol{0}_{\boldsymbol{1:i-1}}^{\boldsymbol{n_k^{F,i}}} \quad \frac{\partial \boldsymbol{h}(\bar{\boldsymbol{x}}^{\boldsymbol{i}})}{\partial \boldsymbol{x}^{\boldsymbol{i}}} \quad \boldsymbol{0}_{\boldsymbol{i+1:N}}^{\boldsymbol{n_k^{F,i}}}\right] \tag{17}$$

is the landmark measurement Jacobian of R_i,

$$\boldsymbol{H_{ij}} = \left[\boldsymbol{0}_{\boldsymbol{1:i-1}}^{\boldsymbol{n_k^{i\to j}}} \quad \boldsymbol{H_i^i} \quad \boldsymbol{0}_{\boldsymbol{i+1:j-1}}^{\boldsymbol{n_k^{i\to j}}} \quad \boldsymbol{H_i^j} \quad \boldsymbol{0}_{\boldsymbol{j+1:N}}^{\boldsymbol{n_k^{i\to j}}}\right] \tag{18}$$

is the relative measurement Jacobian of R_i observing the relative pose of R_j, where $0_{a:b}^c \in \mathbb{R}^{c\times m(b-a+\mathbb{1})}, {H_i}^i = \partial h^{i\to j}\left(\bar{x}^i, \bar{x}^j\right) / \partial x^i\$$, and $H_j^i = \partial h^{I\to j}\left(\bar{x}^i, \bar{x}^j\right) / \partial x^j$. Note that the measurement update step can be processed even if some of the robots in the system could not obtain measurements.

The covariance of the state evolution disturbance and the measurement noise in the joint form are: $W = diag\left(W^1, \cdots, W^i, \cdots, W^N\right)$ and $V = diag\left(\cdots, V^i, \cdots, V^{i\to j}, \cdots\right)$.

The subscript k is omitted to lighten notations.

Discorrelated Minimum Variance

In this report, the Discorrelated Minimum Variance (DMV) [A23, A24] is applied to the relative measurement update steps of the decentralized system's estimation process. Although the method's estimation performance is not as accurate as the CEKF, the method is compatible with integrity monitoring since the approach explicitly bounds the unknown inter-robot correlations, like Covariance Intersection (CI) [A17].

For the prediction step and the landmark measurement update step, an EKF is deployed for each robot in $\mathcal{R}$:

$$\bar{\boldsymbol{x}}_k^i = \boldsymbol{g}\left(\hat{\boldsymbol{x}}_{k-1}^i, \boldsymbol{u_{k-1}^i}\right) \tag{19}$$

$$\bar{\boldsymbol{P}}_{i,k} = \boldsymbol{G_{i,k}}\hat{\boldsymbol{P}}_{i,k-1}\boldsymbol{G_{i,k}^T} + \boldsymbol{W_k^i} \tag{20}$$

$$\widehat{\boldsymbol{x}}_k^{i,LM} = \bar{\boldsymbol{x}}_k^i + \boldsymbol{K}_k^{\boldsymbol{LM}} \boldsymbol{\gamma}_k^{\boldsymbol{i}} \tag{21}$$

$$\widehat{\boldsymbol{P}}_{i,k}^{LM} = \left(\boldsymbol{I} - \boldsymbol{K}_k^{\boldsymbol{LM}} \boldsymbol{H}_k^{\boldsymbol{i}}\right) \overline{\boldsymbol{P}}_{i,k} \tag{22}$$

where $\gamma_k^i = z_k^i - h(\bar{x}_k^i)$, $K_k^{LM} = \bar{P}_{i,k} H_k^{i^T} Y^{LM^{-1}}$, $Y^{LM} = H_k^I \bar{P}_{i,k} H_k^{i^T} + V_k^i$, and $H_k^i = \partial h(\bar{x}_k^i) / \partial x^i$. The superscript LM represents that the variables are obtained after landmark measurement update step. When R_i observes R_j, then a relative measurement update step, or a DMV update step, is processed:

$$\widehat{\boldsymbol{x}}_k^{i,DMV} = \widehat{\boldsymbol{x}}_k^i + \boldsymbol{K}_k^{\boldsymbol{DMV}} \boldsymbol{\gamma}_k^{\boldsymbol{I \to j}} \tag{23}$$

$$\widehat{\boldsymbol{P}}_{i,k}^{DMV} = \widehat{\boldsymbol{P}}_{i,k}(\omega_\star^i) \tag{24}$$

$$\boldsymbol{K}_k^{\boldsymbol{DMV}} = \widehat{\boldsymbol{K}}_\star^i(\omega_\star^i) \tag{25}$$

where $\hat{x}_k^i = \hat{x}_k^{i,LM}$ if R_i observes landmarks before the DMV update step, or $\hat{x}_k^i = \bar{x}_k^i$ if not.

The DMV updated covariance and gain are obtained by:

$$\widehat{\boldsymbol{P}}_i(\omega) = \left(\omega(\overline{\boldsymbol{P}}_i)^{-1} + (1-\omega)\boldsymbol{H}_{\boldsymbol{i}}^{\boldsymbol{i}^T}\left(\boldsymbol{H}_{\boldsymbol{j}}^{\boldsymbol{I}}\overline{\boldsymbol{P}}_j\boldsymbol{H}_{\boldsymbol{j}}^{\boldsymbol{i}^T} + \frac{1-\omega}{\gamma}\boldsymbol{V}^{\boldsymbol{I \to j}}\right)^{-1}\boldsymbol{H}_{\boldsymbol{i}}^{\boldsymbol{i}}\right)^{-1} \tag{26}$$

$$\widehat{\boldsymbol{K}}_\star^i(\omega) = \frac{1}{\omega}\overline{\boldsymbol{P}}_i\boldsymbol{H}_{\boldsymbol{i}}^{\boldsymbol{i}^T}\left(\frac{1}{\omega}\boldsymbol{H}_{\boldsymbol{i}}^{\boldsymbol{i}}\overline{\boldsymbol{P}}_i\boldsymbol{H}_{\boldsymbol{i}}^{\boldsymbol{i}^T} + \frac{1}{1-\omega}\boldsymbol{H}_{\boldsymbol{j}}^{\boldsymbol{i}}\overline{\boldsymbol{P}}_j\boldsymbol{H}_{\boldsymbol{j}}^{\boldsymbol{i}^T} + \frac{1}{\gamma}\boldsymbol{V}^{\boldsymbol{i \to j}}\right)^{-1} \tag{27}$$

Here, the subscript k is omitted.

Finally, the optimization parameter $\omega_\star^i$ is calculated by:

$$\omega_\star^i = \underset{0 \le \omega \le 1}{\operatorname{argmin}} \left(\log\det \widehat{\boldsymbol{P}}_i(\omega)\right) \tag{28}$$

Here, γ in (26) and (27) are selected as $\gamma = 1 - \omega$ to ensure convex optimization for (28).

A-4. Estimation error and fault detector distributions

Here, the distribution of the estimation error and fault detector will be discussed in the presence of measurement faults in preparation for the integrity monitoring derivation.

Centralized EKF Estimation Error

The updated estimate is:

$$\begin{aligned} \hat{x}_k &= \bar{x}_k + K_k(z_k - \hat{z}_k) \\ &= \bar{x}_k + K_k(h(x_k) + v_k + f_k - \hat{z}_k) \\ &\approx \bar{x}_k + K_k(H_k(x_k - \bar{x}_k) + v_k + f_k) \end{aligned} \tag{29}$$

Thus,

$$\delta\hat{x}_k \approx (I - K_k H_k)(\bar{x}_k - x_k) + K_k(v_k + f_k) \tag{30}$$

From the prediction step:

$$\begin{aligned} x_k &= g(x_{k-1}, u_{k-1}) + w_{k-1} \\ &\approx \bar{x}_k + G_k(x_{k-1} - \hat{x}_{k-1}) + w_{k-1} \end{aligned} \tag{31}$$

Substituting into (30) yields:

$$\delta\hat{x}_k \approx \underbrace{\underbrace{(\boldsymbol{I} - \boldsymbol{K_k H_k})}_{\boldsymbol{K'_k}}}_{\boldsymbol{K''_k}} (\boldsymbol{G_k}\,\delta\hat{\boldsymbol{x}}_{k-1} - \boldsymbol{w_{k-1}}) - K_k(v_k + f_k)$$

$$= K''_k \delta\hat{x}_{k-1} - K'_k w_{k-1} + K_k(v_k + f_k) \tag{32}$$

Taking the expectation gives:

$$\mathbb{E}[\delta\hat{x}_k] = f_{\hat{x}_k} \approx K''_k f_{\hat{x}_{k-1}} + K_k f_k \tag{33}$$

$$= \underbrace{[K_k \quad K''_k]}_{A_k} \underbrace{[f_k^T \quad f_{\hat{x}_{k-1}}^T]^T}_{\bar{f}_k} \tag{34}$$

To be conservative, we assume the prior estimate may be faulted (i.e., $f_{\hat{x}_{k-1}}$ may be non-zero) but remains at a **consistent** level as defined in [A17]. Each element of the fault vector f_k corresponds to the elements of the joint measurement vector shown in (15). Note that the covariance of $\delta\hat{x}_k$ remains $\hat{P}_k$, even if faults exist in measurements and prior estimates.

Centralized EKF Fault Detector

Without collaboration, a robot's fault detector is constructed using only its own innovation:

$$q_k^i = \gamma_k^{i^T} Y_k^{i^{-1}} \gamma_k^i \tag{35}$$

Once R_i collaborates with R_j, both the measurements and prior estimate of R_j become correlated with R_i's state estimate. Therefore, a common fault detector is used across all collaborating robots to account for these correlations:

$$q_k^i = q_k^j = \gamma_k^{ij^T} Y_k^{ij^{-1}} \gamma_k^{ij} \tag{36}$$

where γ_k^{ij} is the joint innovation of R_i and R_j, and Y_k^{ij} is its covariance. This common fault detector is used even after the robots stop collaborating to rigorously bound inter-robot cross correlation even if it has small impact on another robot's estimation.

The general form of the joint innovation vector is:

$$\gamma_k = z_k - h(\bar{x}_k)$$

$$\approx H_k(G_k(x_{k-1} - \hat{x}_{k-1}) + w_{k-1}) + v_k + f_k \tag{37}$$

Taking the expectation yields:

$$\mathbb{E}[\gamma_k] = -H_k G_k f_{\hat{x}_{k-1}} + f_k \tag{38}$$

Since γ_k is normally distributed, q_k in the presence of a fault follows a non-central chi-squared distribution:

$$q_k \sim \chi^2_{n_k,\lambda_k}$$

where $\chi^2_{a,b}$ is the chi-squared distribution with a DOF and non-centrality parameter b, n_k is the dimension of the joint innovation vector, and λ_k is the non-centrality parameter:

$$\lambda_k = \mathbb{E}[\gamma_k]^T Y^{-1} \mathbb{E}[\gamma_k]$$

$$= \underbrace{\bar{f}_k^T [I \quad -H_k G_k]^T Y^{-1} \underbrace{[I \quad -H_k G_k]}_{B_k} \bar{f}_k}_{M_k} \tag{39}$$

Lastly, the fault detector threshold T_{D_k} is determined by:

$$T_{D_k} = X_{n_k}^{-2}[1-\alpha] \tag{40}$$

where X_a^{-2} is the inverse cumulative distribution function of the chi-squared distribution with a DOF, and α is the fault detection's predefined false negative probability. Each set of collaborating robots uses the corresponding common q_k and T_{D_k}.

Discorrelated Minimum Variance Estimation Error

If the relative measurement update is performed after the landmark measurement update, then, similar to (29), R_i's state estimate error after the DMV update step becomes:

$$\begin{aligned}\hat{x}_k^{i,DMV} &= \hat{x}_k^{i,LM} + K_k^{DMV}\left(z_k^{I\to j} - \hat{z}_k^{I\to j}\right) \\ &\approx \hat{x}_k^{i,LM} + K_k^{DMV}\left(H_{i,k}^i\left(x_k^i - \hat{x}_k^{i,LM}\right) + H_{j,k}^i\left(x_k^j - \hat{x}_k^j\right) + v_k^{I\to j} + f_k^{i\to j}\right)\end{aligned} \tag{41}$$

which yields:

$$\delta\hat{x}_k^{i,DMV} = \left(I - K_k^{DMV}H_{i,k}^i\right)\left(\hat{x}_k^{i,LM} - x_k^i\right) + K_k^{DMV}H_{j,k}^i\left(x_k^j - \hat{x}_k^j\right) + K_k^{DMV}\left(v_k^{i\to j} + f_k^{i\to j}\right) \tag{42}$$

Taking the expectation yields:

$$\begin{aligned}\mathbb{E}\left[\delta\hat{x}_k^{i,DMV}\right] &= f_{\hat{x}_k^{i,DMV}} \\ &= \underbrace{\left(I - K_k^{DMV}H_{i,k}^{i\to j}\right)}_{K_k'^{DMV}} f_{\hat{x}_k^{i,LM}} + K_k^{DMV}\underbrace{\left(-H_{j,k}^{i\to j}f_{\hat{x}_k^{j,LM}} + f_k^{i\to j}\right)}_{\bar{f}_k^{RM}}\end{aligned} \tag{43}$$

Here, as explained in Section 2.1., the other robot's estimation fault, $f_{\hat{x}_k^{j,LM}}$, is not considered in the relative measurement fault. Therefore, $\bar{f}_k^{RM} = f_k^{i\to j}$ is always satisfied.

Like (33), the fault vector after the landmark measurement update step is:

$$f_{\hat{x}_k^{i,LM}} = \underbrace{\underbrace{\left(I - K_k^{LM}H_k^i\right)}_{K_k'^{LM}}G_k}_{K_k''^{LM}} f_{\hat{x}_{k-1}^i} + K_k^{LM}f_k^i \tag{44}$$

Substituting into (43) yields:

$$\begin{aligned}f_{\hat{x}_k^{i,DMV}} &= K_k'^{DMV}K_k^{LM}f_k^i + K_k'^{DMV}K_k''^{LM}f_{\hat{x}_{k-1}^i} + K_k^{DMV}f_k^{i\to j} \\ &= \underbrace{\begin{bmatrix}\mathrm{K_k^{DMV}} & \mathrm{K_{kK_k^{LM}}'^{DMV}} & \mathrm{K_{kK_k''^{LM}}'^{DMV}}\end{bmatrix}}_{\mathrm{A_k}}\underbrace{\begin{bmatrix}\mathrm{f_k^{i\to j}} \\ \mathrm{f_k^i} \\ \mathrm{f_{\hat{x}_{k-1}^i}}\end{bmatrix}}_{\bar{f}_k}\end{aligned} \tag{45}$$

Discorrelated Minimum Variance Fault Detector

Similar to (35), the decentralized fault detector is constructed using only an individual robot's weighted norm of its innovation:

$$q_k^i = \gamma_k^T Y_k^{-1}\gamma_k \tag{46}$$

where $\gamma_k = \begin{bmatrix}\gamma_k^{i\to j^T} & \gamma_k^{i^T}\end{bmatrix}^T$ and Y_k is its covariance matrix (Note that the DMV's innovation vector order differs from the CEKF since the relative measurement update is performed after the landmark measurement

update). The dimension of γ_k increases as the number of robots observed by R_i increases. For simplicity, we assume the case where only the relative measurement from R_i to R_j is obtained.

The innovation vector of the relative measurement is expressed as:

$$\begin{aligned}\gamma_k^{i\to j} &= z_k^{i\to j} - h^{i\to j}\left(\hat{x}_k^{i,LM}, \hat{x}_k^{j}\right) \\ &\approx H_{i,k}^{i}\left(x_k^i - \hat{x}_k^{i,LM}\right) + H_{j,k}^{i}\left(x_k^j - \hat{x}_k^j\right) + v_k^{i\to j} + f_k^{i\to j}\end{aligned} \tag{47}$$

Taking the expectation while assuming no R_j estimation fault:

$$\mathbb{E}\left[\gamma_k^{i\to j}\right] = -H_{i,k}^{i} f_{\hat{x}_k^{i,LM}} - \boxed{H_{j,k}^{i} f_{\hat{x}_k^{j,LM}}} + f_k^{i\to j} \tag{48}$$

$$= -H_{i,k}^{i} K_k^{\prime\prime LM} f_{\hat{x}_{k-1}^{i}} - H_{i,k}^{i} K_k^{LM} f_k^i + f_k^{i\to j} \tag{49}$$

$$= \begin{bmatrix} I & -H_{i,k}^{i} K_k^{LM} & -H_{i,k}^{i} K_k^{\prime\prime LM} \end{bmatrix} \underbrace{\begin{bmatrix} f_k^{i\to j} \\ f_k^i \\ f_{\hat{x}_{k-1}^{i}} \end{bmatrix}}_{\bar{f}_k} \tag{50}$$

Here, as explained in Section 4.2.1., $\boldsymbol{f}_{\hat{\boldsymbol{x}}_{\boldsymbol{k}}^{\boldsymbol{j,LM}}}$ is assumed to be zero. Similarly, as in (38), the expectation of γ_k^i is:

$$\mathbb{E}\left[\gamma_k^i\right] = -H_k^i G_{i,k} f_{\hat{x}_{k-1}^{i}} + f_k^i \tag{51}$$

Thus, the expectation of γ_k becomes:

$$\mathbb{E}[\gamma_k] = \underbrace{\begin{bmatrix} I & -H_{i,k}^{i} K_k^{LM} & -H_{i,k}^{i} K_k^{\prime\prime LM} \\ 0 & I & -H_k^i G_{i,k} \end{bmatrix}}_{B_k} \bar{f}_k \tag{52}$$

Finally, q_k^i follows:

$$q_k^i \sim \chi^2_{n_k,\lambda_k} \tag{53}$$

where n_k is the dimension ofγ_k and $\lambda_k = \bar{f}_k^T \underbrace{B_k^T Y_k^{-1} B_k}_{M_k} \bar{f}_k$.

A-5. Integrity Monitoring

As shown in the previous sections, the distributions of the estimation error and the fault detector can be generalized as:

$$\delta\hat{x}_k \sim \mathcal{N}\left(A_k \bar{f}_k, \hat{P}_k\right) \tag{54}$$

$$q_k \sim \chi^2_{n_k,\lambda_k} \tag{55}$$

where A_k, $\bar{f}_k$, n_k, and M_k in λ_k were defined differently for two estimators in Section 4. The worst-case fault that maximizes the integrity risk under each fault hypothesis is derived to upper bound the integrity risk. Since each innovation vector and estimation error are independent [25]:

$$P(HMI_k|H_h) = P(|\delta\hat{x}_k| > l|H_h) P\left(q_k < T_{D_K}\middle|H_h\right) \tag{56}$$

The worst-case fault η that maximizes the integrity risk is:

$$\eta = \underset{f}{\operatorname{argmax}}\, P(|\delta\hat{x}| > l|H_h)P(q < T_D|H_h) \tag{57}$$

The worst-case fault's direction is in the direction that maximizes the failure mode slope [26], the ratio of the estimation error's squared mean and the fault detector's non-centrality parameter, $f_{\hat{x}_k}^2/\lambda_k$. [A25] proved this to be:

$$\eta_{dir} = E_h^T\left[E_h M E_h^T\right]^{-1} E_h A^T t \tag{58}$$

where t extracts the element of the robot's state of interest, such as the robot's heading direction or cross-track direction, and E_h extracts the corresponding faulted elements under hypothesis H_h (see [A6] for a detailed explanation). Given the worst-case direction, its magnitude is obtained by:

$$\eta_{mag} = \underset{y}{\operatorname{argmax}}\, P\left(\left|Z_{y\check{f}_{\hat{x}},\hat{\sigma}^2}\right| > l\right) X^2_{n_z,y^2\check{\lambda}}[T_D] \tag{59}$$

where $Z_{a,b}$ is a random Gaussian variable with mean a and variance b, and $X^2_{c,d}[\cdot]$ is the cummulative distribution function of the chi-square distribution with c DOF and non-centrality parameter d. Also, $\check{f}_{\hat{x}} = t^T A\eta_{dir}$ and $\check{\lambda} = \eta_{dir}^T M \eta_{dir}$. Finally, the upper bound of the integrity risk under each hypothesis is obtained by substituting η_{dir} and η_{mag} into (57).

A-6. Performance Evaluation

Simulation

Two simulated collaborating homogeneous robots move in parallel from left to right, collecting measurements and simultaneously update their estimates (see Fig. A1 and Table A1). Fig. A2 compares the 3σ envelope of robots' position estimates along heading direction, while Fig. A3 compares the integrity risk.

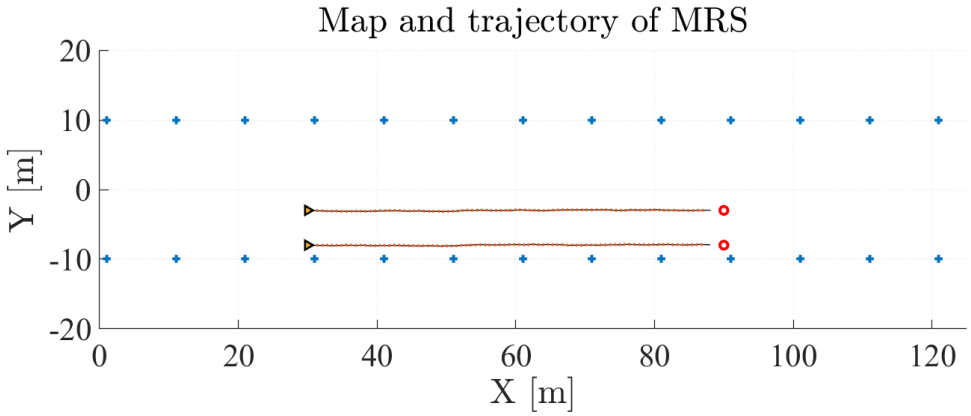

Fig.A 1. Simulated landmark map. Two robots are collaborating throughout the entire operation. The sampling rate for all sensors is 0.1*s.*

lidar SD	lidar range	RM SD	velocity SD	steering SD
0.3 m	20 m	0.1 m	0.5 m/s	5°

Table A1. Sensor parameters used in the simulation.

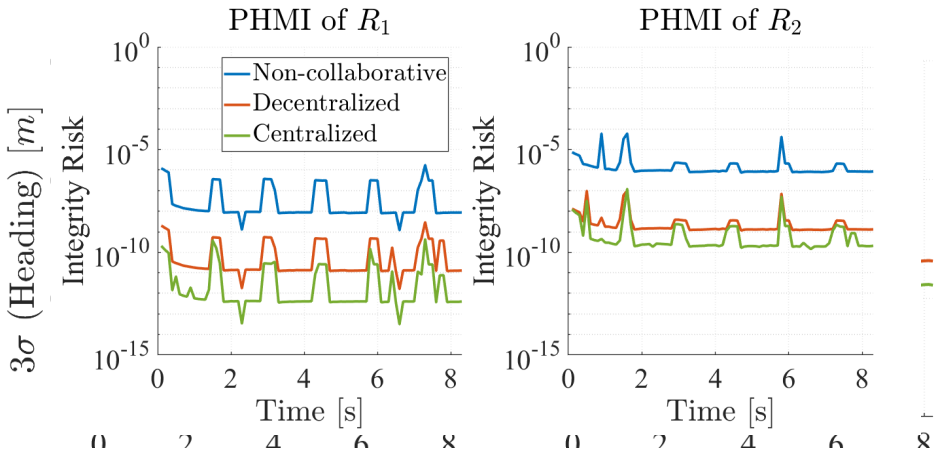

Fig. A4. Integrity risk results of the simulation. The alert limit $l = 0.5\ m$ and $\alpha = 0.1$ are selected for both robots.

Fig. A2. 3σ envelope of robots' state of interest, with the robots' heading direction selected.

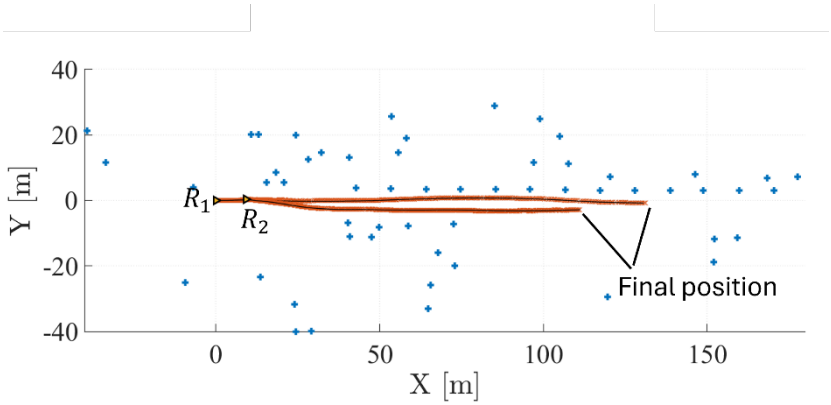

Fig. A3. Experiment landmark map. Two robots move from left to right.

The CEKF shows a lower integrity risk than the non-collaborative EKF because the CEKF benefits from relative measurements, which results in more accurate estimations compared to the EKF. Although the DMV does not improve estimation accuracy beyond the EKF, it has better integrity risk due to the additional measurements provided by the relative measurement, which enhance the fault detection performance. Overall, the simulations demonstrate that collaboration can improve estimation accuracy and reduce integrity risk.

Experiment

Two vehicles collected data on the Illinois Tech campus to experimentally evaluate integrity risk. Each vehicle was equipped with a STIM-300 tactical-grade IMU, an Ouster OS1-64 lidar, and a Novatel GNSS receiver. The IMU readings were used as control inputs. The lidars detected landmarks (e.g., tree trunks and light posts) and measured the vehicles' relative positioning via reflective tape placed on each vehicle. The GNSS clock synchronized the timing of measurements between the vehicles.

Vehicle pose ground truth was obtained by scan matching. The experimental map was generated by merging the maps created by each vehicle using EKF-SLAM (see Fig. A4). Initially, R_1 was behind R_2, but midway through the operation R_1 overtook R_2.

Fig. A5. Vehicles used to collect experimental data. Each vehicle is equipped with NOVATEL GNSS receiver, OS1-64 LiDAR, and STIM 300 tactical grade IMU. Relative pose measurements are obtained by detecting retroreflective tape attached on each sensor suit mounted on each vehicle.

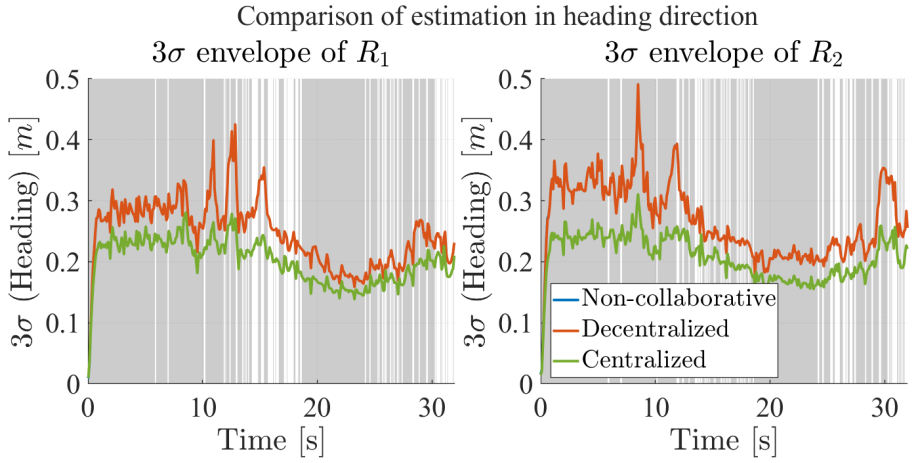

Fig. A6. 3σ envelope of robots' state of interest, with the robots' heading direction selected. Gray shaded areas indicate the times when each robot received relative measurement and collaboratively localized.

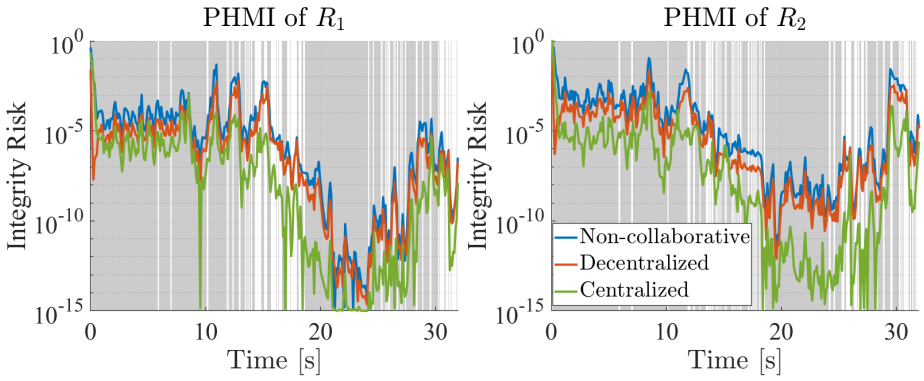

Fig. A7. Integrity risk results of the experiment. The alert limit $l = 0.5\ m$ and $\alpha = 0.1$ are selected for both robots.

Fig. A6 compares the 3σ envelope of the robots' position estimation along the heading direction for each estimator, while Fig. A7 compares the integrity risk; gray areas indicate when the robots observed each other.

The experimental results align with the simulation results. The CEKF demonstrates better estimation accuracy and lower integrity risk than both the EKF and the DMV. Although the DMV did not improve estimation accuracy, it still exhibited better integrity risk than the non-collaborative EKF. Overall, the experimental findings confirm that collaborative localization can improve estimation accuracy and reduce integrity risk.

In both experiments and simulations, although the CEKF shows superior estimation accuracy to the DMV, its improvement in integrity risk is marginal. This is because the landmark measurements from other robots are nearly uncorrelated with the ego robot's state estimate, diminishing the performance of the common fault detector.

A-7. Conclusions

Both simulation and experimental results demonstrate that the CEKF has a lower integrity risk than the non-collaborative EKF. This is due to the CEKF's enhanced estimation accuracy, and the additional measurements provided by collaborating robots, which improve fault detection performance, though there is still room for further improvement. While the DMV does not improve estimation accuracy, its integrity risk is lower than that of the EKF in both simulations and experiments. This is because the DMV fault detector performs better than the EKF by utilizing relative measurements that are not available in the EKF. In summary, collaborative localization enhances integrity risk performance and provides safer navigation compared to standalone robots.

References

[A1] S. Zhang, J. Shan, and Y. Liu, "Variational bayesian estimator for mobile robot localization with unknown noise covariance," IEEE/ASME Transactions on Mechatronics, vol. 27, no. 4, pp. 2185–2193, 2022.

[A2] V. Venkatasubramanian, R. Rengaswamy, K. Yin, and S. N. Kavuri, "A review of process fault detection and diagnosis: Part i: Quantitative model-based methods," Computers & chemical engineering, vol. 27, no. 3, pp. 293–311, 2003.

[A3] B. W. Parkinson and P. Axelrad, "Autonomous gps integrity monitoring using the pseudorange residual," Navigation, vol. 35, no. 2, pp. 255–274, 1988.

[A4] M. Joerger and B. Pervan, "Kalman filter-based integrity monitoring against sensor faults," Journal of Guidance, Control, and Dynamics, vol. 36, no. 2, pp. 349–361, 2013.

[A5] H. Jiang, T. Li, D. Song, and C. Shi, "An effective integrity monitoring scheme for gnss/ins/vision integration based on error state ekf model," IEEE Sensors Journal, vol. 22, no. 7, pp. 7063–7073, 2022.

[A6] G. D. Arana et al., "Recursive integrity monitoring for mobile robot localization safety," in IEEE ICRA, 2019, pp. 305–311.

[A7] A. Hassani, N. Morris, M. Spenko, and M. Joerger, "Experimental integrity evaluation of tightly-integrated imu/lidar including return-light intensity data," in Proceedings of the 32nd International Technical Meeting of The Satellite Division of the Institute of Navigation (ION GNSS+ 2019), 2019, pp. 2637–2658.

[A8] O. A. Hafez, G. D. Arana, M. Joerger, and M. Spenko, "Quantifying robot localization safety: A new integrity monitoring method for fixed-lag smoothing," IEEE Robotics and Automation Letters, vol. 5, no. 2, pp. 3182–3189, 2020.

[A9] O. A. Hafez, M. Joerger, and M. Spenko, "How safe is particle filtering-based localization for mobile robots? an integrity monitoring approach," IEEE Transactions on Robotics, 2024.

[A10] J. Rife, “Collaboration-enhanced receiver integrity monitoring with common residual estimation,” in Proceedings of the 2012 IEEE/ION Position, Location and Navigation Symposium. IEEE, 2012, pp. 1042–1053.

[A11] J. Xiong, J. W. Cheong, Z. Xiong, A. G. Dempster, S. Tian, and R. Wang, “Integrity for multi-sensor cooperative positioning,” IEEE Transactions on Intelligent Transportation Systems, vol. 22, no. 2, pp. 792–807, 2019.

[A12] H. Jing, Y. Gao, S. Shahbeigi, and M. Dianati, “Integrity monitoring of gnss/ins based positioning systems for autonomous vehicles: State-of-the-art and open challenges,” IEEE Transactions on Intelligent Transportation Systems, vol. 23, no. 9, pp. 14 166–14 187, 2022.

[A13] J. He, Z. Tang, X. Fu, S. Leng, F. Wu, K. Huang, J. Huang, J. Zhang, Y. Zhang, A. Radford et al., “Cooperative connected autonomous vehicles (cav): research, applications and challenges,” in 2019 IEEE 27th International Conference on Network Protocols (ICNP). IEEE, 2019, pp. 1–6.

[A14] J. Yin, T. ElBatt, G. Yeung, B. Ryu, S. Habermas, H. Krishnan, and T. Talty, “Performance evaluation of safety applications over dsrc vehicular ad hoc networks,” in Proceedings of the 1st ACM international workshop on Vehicular ad hoc networks, 2004, pp. 1–9.

[A15] A. Petrillo, A. Pescape, and S. Santini, “A secure adaptive control for cooperative driving of autonomous connected vehicles in the presence of heterogeneous communication delays and cyberattacks,” IEEE transactions on cybernetics, vol. 51, no. 3, pp. 1134–1149, 2020.

[A16] S. Leonardos and K. Daniilidis, “A game-theoretic approach to robust fusion and kalman filtering under unknown correlations,” in 2017 american control conference (acc). IEEE, 2017, pp. 2568–2573.

[A17] S. J. Julier and J. K. Uhlmann, “A non-divergent estimation algorithm in the presence of unknown correlations,” in Proceedings of the 1997 American Control Conference (Cat. No. 97CH36041), vol. 4. IEEE, 1997, pp. 2369–2373.

[A18] S. Huang and G. Dissanayake, “Convergence and consistency analysis for extended kalman filter based slam,” IEEE Transactions on robotics, vol. 23, no. 5, pp. 1036–1049, 2007.

[A19] G. P. Huang, N. Trawny, A. I. Mourikis, and S. I. Roumeliotis, “Observability-based consistent ekf estimators for multi-robot cooperative localization,” Autonomous Robots, vol. 30, pp. 99–122, 2011.

[A20] G. D. Arana et al., “Efficient integrity monitoring for kf-based localization,” in IEEE ICRA, 2019.

[A21] A. Prorok, A. Bahr, and A. Martinoli, “Low-cost collaborative localization for large-scale multi-robot systems,” in 2012 IEEE International Conference on Robotics and Automation. Ieee, 2012, pp. 4236–4241.

[A22] S. Thrun, “Probabilistic robotics,” Communications of the ACM, vol. 45, no. 3, pp. 52–57, 2002.

[A23] J. Zhu and S. S. Kia, “Cooperative localization under limited connectivity,” IEEE Transactions on Robotics, vol. 35, no. 6, pp. 1523–1530, 2019.

[A24] C. Chen and S. S. Kia, “Cooperative localization using learning-based constrained optimization,” IEEE Robotics and Automation Letters, vol. 7, no. 3, pp. 7052–7058, 2022.

[A25] M. Joerger, F.-C. Chan, and B. Pervan, “Solution separation versus residual-based raim,” NAVIGATION: Journal of the Institute of Navigation, vol. 61, no. 4, pp. 273–291, 2014.

[A26] J. Angus, “Raim with multiple faults,” Navigation, pp. 249–257, 2006.